



Significant Enhanced Optical Parameters of PVA-Y₂O₃ Polymer Nanocomposite Films

Z. A. Alrowaili¹ · T. A. Taha^{2,3} · Karam S. El-Nasser^{4,5} · Hossam Donya^{6,7}

Received: 10 December 2020 / Accepted: 17 February 2021 / Published online: 10 April 2021
© The Author(s), under exclusive licence to Springer Science+Business Media, LLC, part of Springer Nature 2021

Abstract

In our present work, PVA-Y₂O₃ nanocomposite films were prepared based on solution casting technique. The structures of the nanocomposite films were examined by XRD and FTIR spectroscopy. From the XRD analysis, it is found that the films are semi-crystalline and Y₂O₃ nanoparticles have cubic crystal structure. The average crystal size estimated via Scherer formula was 25 nm while W–H plot method gives 28 nm. FTIR spectra of all nanocomposite films exhibited good interaction between nano-Y₂O₃ and the PVA network. The morphological images obtained from SEM microscopy indicated good distribution of nano-Y₂O₃. Optical absorption spectra of the films enhanced with the incorporation of Y₂O₃. As the percentage of Y₂O₃ added increased, the direct optical energy gap, decreased from 5.42 to 5.31 eV. While the static refractive index, dispersion energy, third order optical susceptibility, nonlinear refractive index and optical conductivity increased.

Keywords PVA nanocomposites · Refractive index · Optical susceptibility · Optical conductivity

1 Introduction

Nowadays with the rapid advancement of nanoscience and technology, extensive research and development implemented on high performance polymeric nanomaterials for targeted applications in various fields [1–3]. The incorporation of nanoscale reinforcements into the polymer matrix is also an endeavor to develop polymer nanocomposites in

different scientific and industrial fields [4–7]. Polyvinyl alcohol (PVA) features high elasticity, transparency and excellent relaxation properties therefore, selected for preparing PVA hybrid nanocomposites [8–12]. Because of its high refractive index, large energy gap and low phonon energy, barium Y₂O₃ is an important ceramic to be applied as the inorganic filler in polymer nanocomposites [13–15]. By varying the loading concentration, polymer nanocomposites would also enable the fine tuning of refractive index and the realization of grade-index structure.

Optical properties of PVA/iron oxide nanoparticles have been investigated [16]. The band gaps decrease as the concentration of iron oxide increases and the refractive index enhanced as well. In the fluorescence spectra three peaks observed at 421, 451 and 469 nm. Chahal et al. [17] have demonstrated the effect of irradiation on the optical properties of PVA-Ag nanocomposites. Accordingly, the optical band gap decreased from 4.57 to 3.05 eV. These nanocomposites showed high ability to block UV radiation. Morad et al. [18] have studied PVA as the matrix for dispersing different phases of TiO₂ nanoparticles. The optical band gap changed from 3.25 to 2.63 eV as the TiO₂ changed from anatase to rutile. It was found that the optical conductivity of PVA-TiO₂ (anatase) is higher than that for PVA-TiO₂ (rutile). M. Rashad [19] considered PVA polymer matrix loaded with Fe₂O₃ and NiO nanoparticles. It is found that the addition

✉ T. A. Taha
taha.hemida@yahoo.com

¹ Physics Department, College of Science, Jouf University, P.O.Box:2014, Sakaka, Saudi Arabia

² Physics Department, College of Science and Arts, Jouf University, P.O. Box 756, Al-Gurayyat, Saudi Arabia

³ Physics and Engineering Mathematics Department, Faculty of Electronic Engineering, Menoufia University, Menouf 32952, Egypt

⁴ Chemistry Department, College of Science and Arts, Jouf University, P.O. Box 756, Al-Gurayyat, Saudi Arabia

⁵ Chemistry Department, Faculty of Science, Al-Azhar University, Assiut 71524, Egypt

⁶ Department of Physics, Faculty of Science, King Abdulaziz University, Jeddah 21589, Saudi Arabia

⁷ Physics Department, Faculty of Science, Menoufia University, Shebin El-Koom, Egypt

of both Fe_2O_3 and NiO increased the optical energy gap as well as dispersion energy. At 1.0 wt% of nano- Fe_2O_3 , the static refractive index, third order optical susceptibility and optical conductivity enhanced. PVA-CdS nanocomposites obtained by solution casting route [20]. The UV absorption edge located at 502 nm and a sharp emission peak appeared at 502 nm. After irradiation of PVA-CdS composites, the defect emission quenched. Raju et al. [21] studied the emission spectra of PVA- Eu^{3+} polymer film. The optical absorption spectra indicated an absorption band at 275 nm. After UV irradiation the fluorescence spectra of PVA unchanged while the PVA- Eu^{3+} revealed a red emission. Abdullah et al. [22] have developed PVA/PbS nanocomposites via solution casting and reduction technique. The PbS nanoparticles decreased the energy gap from 6.27 to 2.34 eV. It is found that the static refractive index values ranged from 1.09–1.20 as depicted from Cauchy model. Additionally, the refractive index and optical conductivity of PVA/PbS films enhanced with increasing the concentration of nano-PbS. Heiba et al. [23] prepared PVA-CdSe nanocomposites based on solution casting method. It is found that the optical band gap increased from 5.0 to 5.34 eV with the content of CdSe. Also, the refractive index enhanced with increasing CdSe ratios. As indicated multicolor emission peaks in the UV-Vis spectral region observed with blue shift. PVA-ZnO nanocomposite films have been prepared and their optical properties investigated [24]. As the ZnO content increase the optical band gaps decreased from 4.76 eV to 2.38 eV. Interestingly, the PVA-ZnO nanocomposites showed enhanced UV luminescence at 10 mol% of ZnO.

The development of polymer nanocomposites with tunable optical properties is an active field of research. The grand challenge for the generation of such materials is to develop an integrated synthesis strategy adapting particle generation, surface modification and integration inside the polymer. In the present research, we report the simple synthesis of PVA/ Y_2O_3 nanocomposite films as well as their structural and optical investigations. The structures of the hybrid films were examined by XRD and FTIR measurements. The morphologies of the cross-sectional areas of the films were characterized by SEM. The linear and non-linear optical parameters like refractive index, dispersion energy and non-linear optical susceptibility were analyzed.

2 Experimental Procedure

The films of (PVA- Y_2O_3) nanocomposites in different Y_2O_3 wt% ratios (0.0, 1.0 and 3.0) were prepared by solution cast technique. 1.0 g of PVA dissolved in distilled water and stirred for 1.0 h to obtain a clear and homogeneous solution. A known amount of Y_2O_3 added and stirred continuously

until a viscous solution obtained. The solution was poured into the polystyrene petri dishes to get thin films.

The crystal structure of nanocomposite films was examined by a Rigaku XRD-6000 diffractometer (Cu $\text{K}\alpha$ radiation, $\lambda = 0.15418$ nm). Microscopic study of the PVA- Y_2O_3 surface conducted on a Quattro ESEM's environmental scanning electron microscope (Thermo Fisher Scientific). The FTIR/ATR spectra were recorded for 400–4,000 wavenumber using PerkinElmer100 FTIR spectrometer (USA). Optical measurements were performed using High Precision UV-VIS Spectrophotometer PD-3000UV (Japan), having a dual light source capable of emitting ultraviolet as well as visible light.

3 Results and Discussion

Figure 1 contains measurements of X-ray diffraction for PVA- Y_2O_3 nanocomposite films at different ratios of nano- Y_2O_3 (0.0, 1.0 and 3.0 wt%). It is observed from this figure that the polyvinyl film has a semi-crystalline structure of the monoclinic structure at $2\theta = 18.54^\circ$ which agree with the literature [9]. After doping the PVA films the XRD spectrum showed diffraction lines of nano- Y_2O_3 as well. The spectrum of Y_2O_3 nanopowder match very well with the cubic crystal structure reported in ICDD PDF 41–1105 and agree very well with the data reported in the literature [25, 26]. Numerous studies demonstrated that the Scherrer equation applied to determine the average size of crystals (D) from the XRD patterns [27–37]

$$D = \frac{0.9\lambda}{\beta \cos \theta} \quad (1)$$

where λ is the X-ray wavelength, θ is the diffraction angle and β is the corrected full width at half maximum.

After applying this equation, we obtained an average size for Y_2O_3 nanocrystals of about 25 nm. In view of the importance of applying the Williamson-Hall model to calculate the average size of crystals [38, 39], the linear fitting of data in Fig. 1b was used to calculate the size of Y_2O_3 crystals according to this model (see Fig. 1b). Thus, the average size of the crystals is approximately 28 nm. The microstrain (ϵ) value was 1.05×10^{-3} , which contributed to the broadening of the diffraction peaks and thus the estimated crystal size is larger than that computed from Scherrer formula.

To study the surface morphology of the prepared films, scanning electron microscopy images collected and displayed in Fig. 2. The SEM image of the Y_2O_3 nanopowder showed fine nanoparticles (see Fig. 2a).

Figure 2 shows the SEM images containing a uniform distribution of Y_2O_3 nanoparticles without large agglomerations.

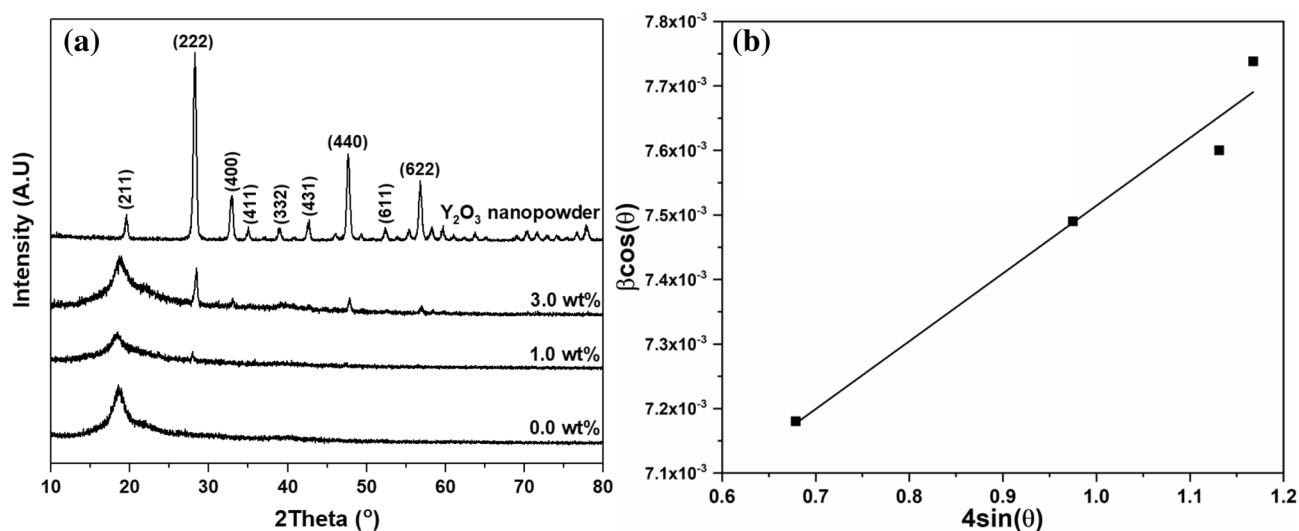


Fig. 1 a XRD spectra of PVA-Y₂O₃ nanocomposites and b βcos(θ) versus 4sin(θ) for Y₂O₃ nanopowder

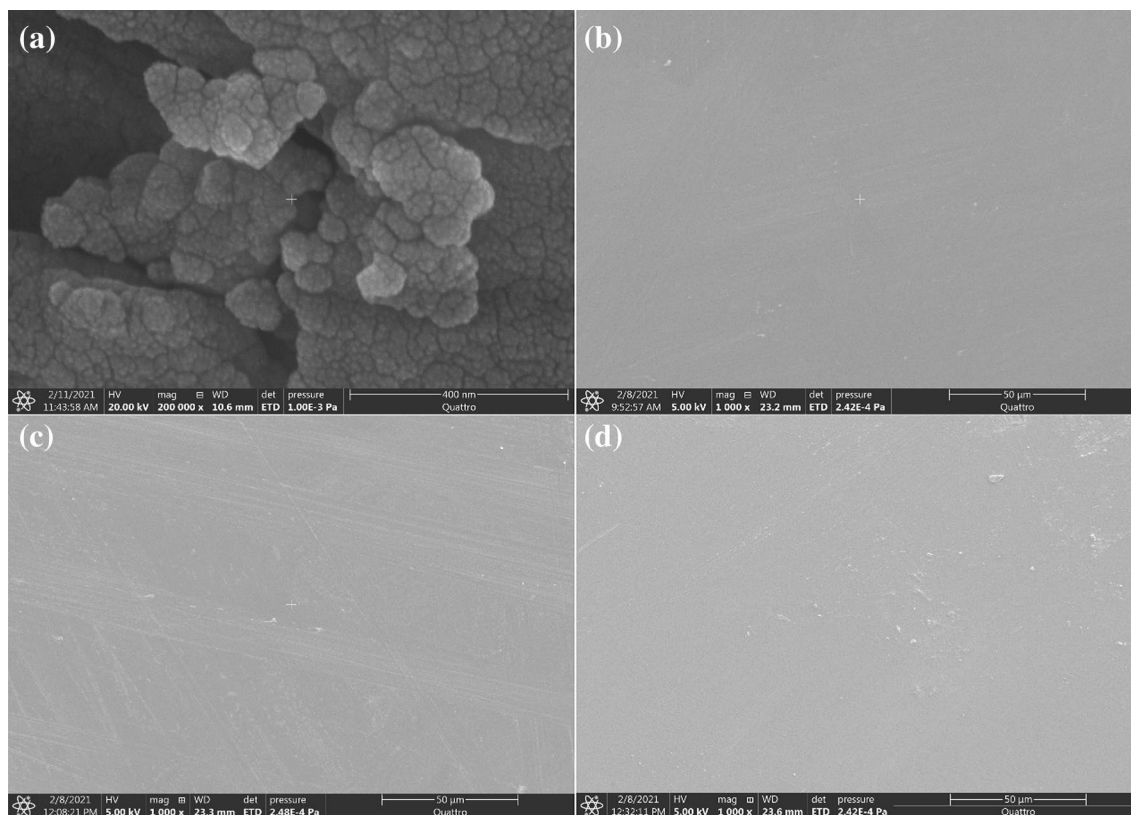


Fig. 2 SEM scans of a Y₂O₃ nanopowder, b PVA pure film, c PVA + 1.0 wt% Y₂O₃ and d PVA + 3.0 wt% Y₂O₃ nanocomposite films

In Fig. 3, the FTIR/ATR spectra of the polyvinyl alcohol films doped with nano-Y₂O₃ at ratios 0.0, 1.0, 3.0 wt%. Looking at this figure, a strong absorption band at 3292 cm⁻¹ that is related to O–H stretching vibrations [9, 40–44]. The transmission bands at 2920 and 2850 cm⁻¹

denote the asymmetrical and symmetrical stretching vibrations of C–H. Two absorption bands appeared at 1716 and 1088 cm⁻¹ comes due to C=O and C–O stretching vibrations of vinyl acetate group. It is evident here that the absorption peak at 1418 cm⁻¹ related to –C–H– [45], shifted to

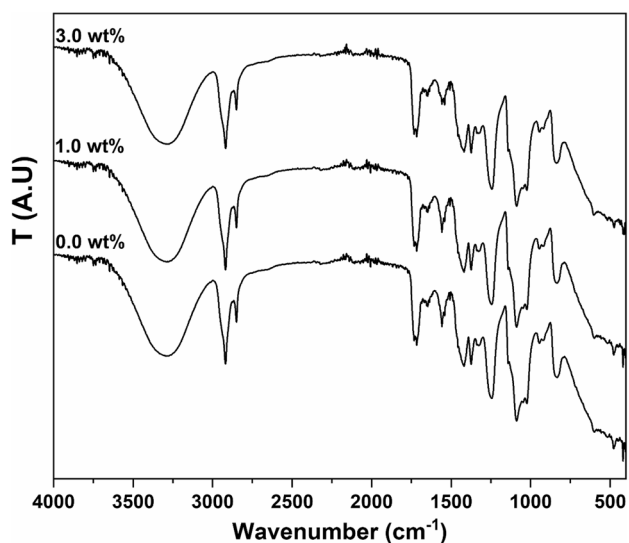


Fig. 3 FTIR/ATR spectra of PVA- Y_2O_3 nanocomposites

1416 cm^{-1} when the ratio of Y_2O_3 was 3.0 wt%. The peak appeared at 1327 cm^{-1} is due to wagging vibrations of C-H groups. The bands at 944 and 833 cm^{-1} correspond to skeletal vibrations of PVA [46]. From the current data, it is apparent that there is a strong intercalation between the polymer vinyl alcohol network and Y_2O_3 nanoparticles.

Figure 4 shows optical data such as absorbance, transmittance and reflectance for the present PVA- Y_2O_3 nanocomposite films. It is clear that increasing the concentration of nano- Y_2O_3 improved the absorbance of the nanocomposite films (Fig. 4a). Also, the optical transmittance decreased due to the increase in Y_2O_3 concentration (Fig. 4b).

Also in Fig. 4a an absorption peak at 280 nm noticed, which is associated with $n-\pi^*$ transition of $C=O$ [47]. From

the figure, it is observed that when the loading of Y_2O_3 increases, the intensity of this peak enhanced.

The direct and indirect optical energy gaps can be determined by applying the Tauc's equation to the optical absorption data [48, 49];

$$\alpha h\nu = B(h\nu - E_g)^n \quad (2)$$

where α denotes the optical absorption, $h\nu$ is the energy of the photon beam, B is a constant and n equals 0.5 for direct allowed transitions but $n = 2.0$ in case of indirect allowed transitions. Figure 5 shows a graph between $(\alpha h\nu)^n$ vs. $h\nu$ for the nanocomposite films. From this figure, the direct ($E_{g(\text{direct})}$) and indirect ($E_{g(\text{indirect})}$) energy gaps can be estimated via extrapolating the linear part to zero photon absorption ($(\alpha h\nu)^n = 0$). The estimated values of $E_{g(\text{direct})}$ are 5.42, 5.37 and 5.31 eV when the Y_2O_3 percentage is 0.0, 1.0 and 3.0 wt%, respectively. It is found that the samples have indirect energy gaps (4.90, 4.73 and 4.54 eV) for the concentrations 0.0, 1.0 and 3.0 wt% of nano- Y_2O_3 . The decrease of both energy gaps with addition of nano- Y_2O_3 may be due the formation of new levels [39].

It was demonstrated in the previous work that the linear refractive index (n) can be estimated from the following relation [39, 50]:

$$n = \left(\frac{1+R}{1-R} \right) + \sqrt{\frac{4R}{(1-R)^2} - k^2}, \quad k = \frac{\alpha\lambda}{4\pi} \quad (3)$$

where R denotes reflectance and k is the extinction coefficient.

Figure 6 shows the linear refractive index profiles for PVA- Y_2O_3 films when the PVA matrix doped with 0.0, 1.0 and 3.0 wt% of Y_2O_3 . It is apparent that the refractive index enhanced

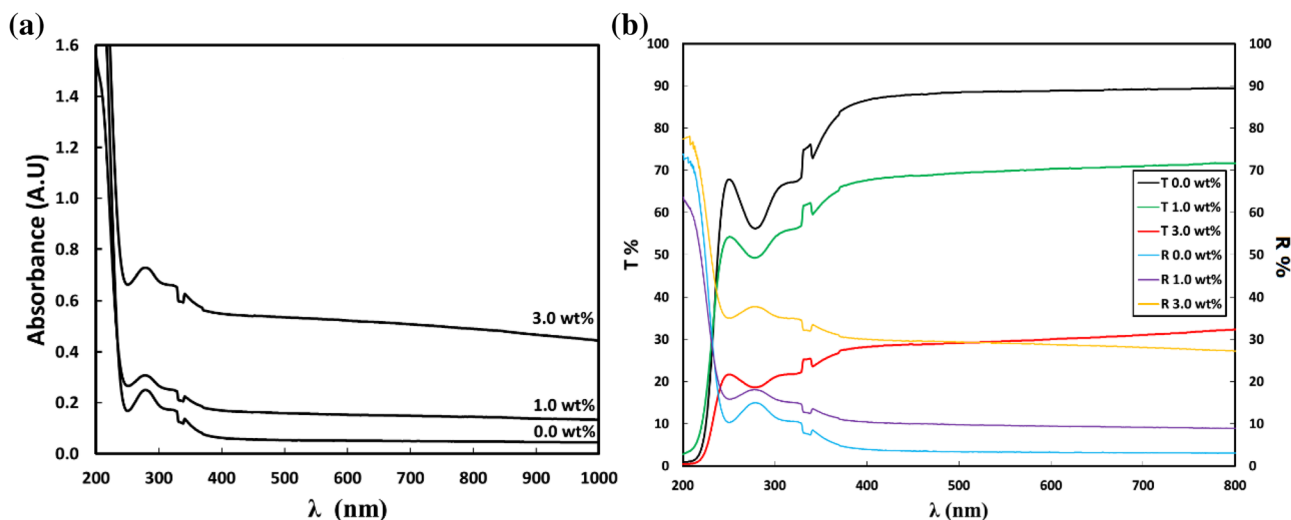


Fig. 4 Optical absorbance, transmittance and reflectance data for the PVA- Y_2O_3 nanocomposites

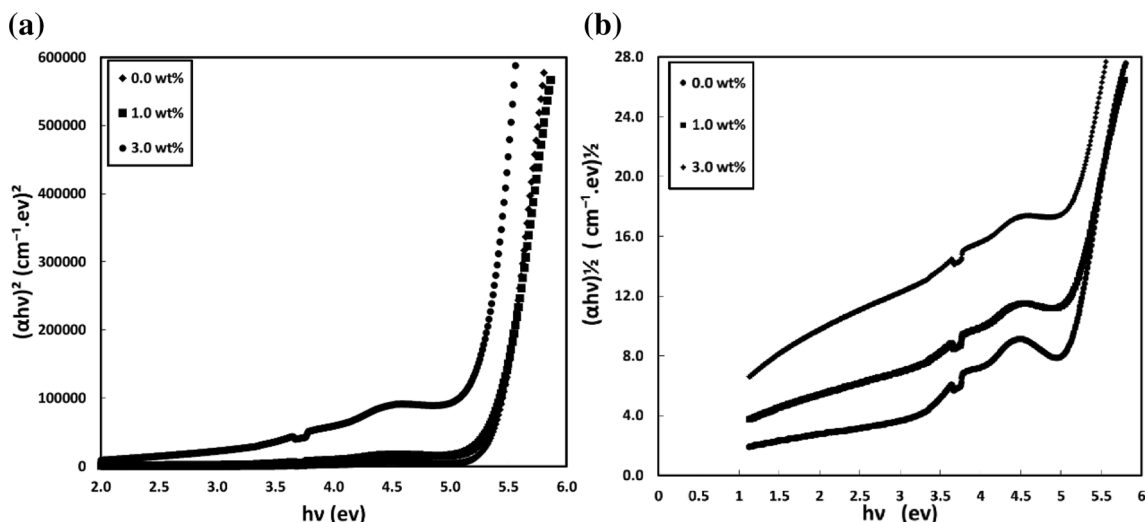
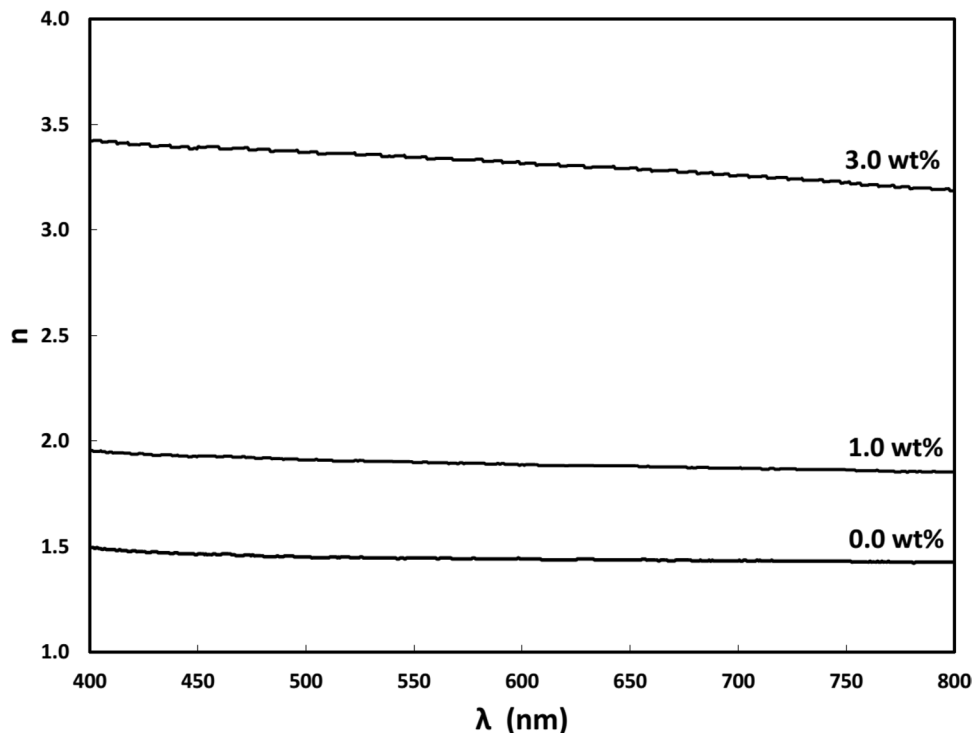


Fig. 5 a $(\alpha h\nu)^2$ and b $(\alpha h\nu)^{0.5}$ as a function of $h\nu$ for the PVA- Y_2O_3 nanocomposite films

Fig. 6 Variation of linear refractive index versus wavelength for the PVA- Y_2O_3 nanocomposite films



when the ratios of nano- Y_2O_3 increased up to 3.0 wt%. This increase in the linear refractive index is due to the agglomeration of particles and therefore increasing the dispersion of the nanocomposite films [39].

It is known that the refractive index dispersion is defined as [51];

$$(n^2 - 1)^{-1} = \frac{E_0}{E_d} - \frac{1}{E_0 E_d} (h\nu)^2, \tag{4}$$

where E_0 denotes the single oscillator energy and E_d measures the interband optical transition strength (dispersion energy). Figure 7 shows the graphs of $(n^2 - 1)^{-1}$ versus $(h\nu)^2$, which gives straight lines.

In Fig. 7, the slope of the straight lines equals $\left(-\frac{1}{E_0 E_d}\right)$ and the intercept is (E_0/E_d) . Table 1, gives the estimated values of E_0 and E_d for the PVA- Y_2O_3 nanocomposite films. It is noted here that the single oscillator energy decreased from 4.15 to 2.91 eV while the dispersion energy increased

Fig. 7 The graphs of $(n^2 - 1)^{-1}$ versus $(h\nu)^2$ for the PVA-Y₂O₃ nanocomposite films

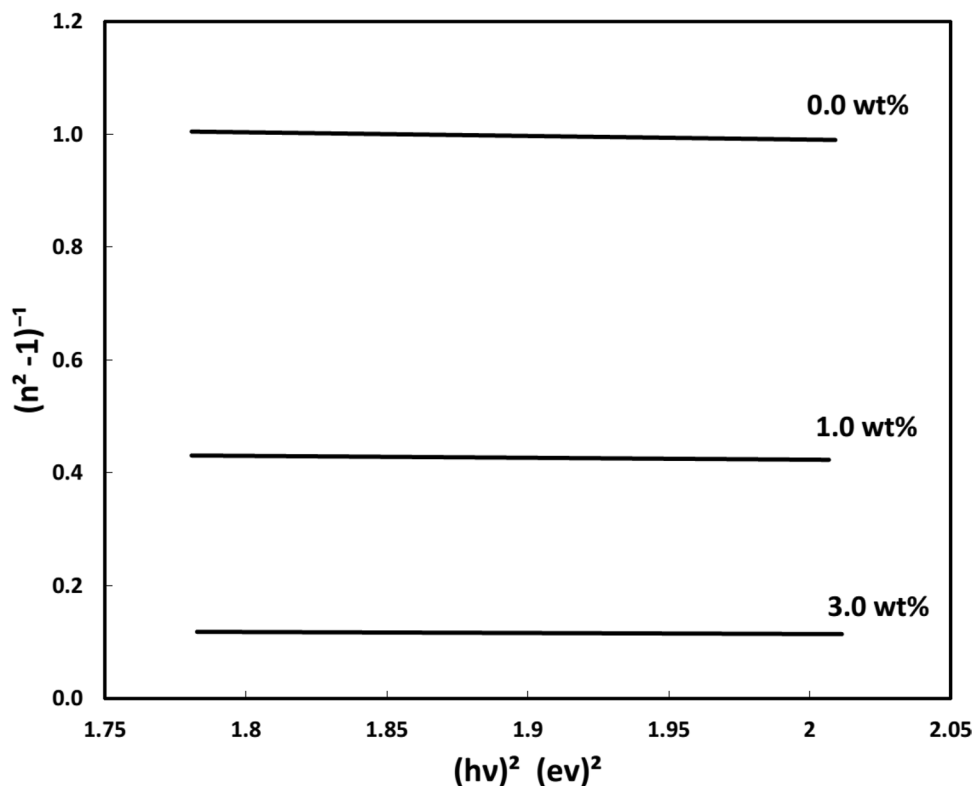


Table 1 Estimated values of E_0 , E_d and static refractive index (n_0) for the PVA-Y₂O₃ nanocomposite films

O ₃ content (wt%)	E_0 (eV)	E_d (eV)	n_0	f (eV ²)	$\chi^{(1)} \times 10^{-3}$	$x^{(3)} \times 10^{-15}$ (e.s.u)	$n_2 \times 10^{-11}$ (e.s.u)
0.0	4.15	3.70	1.38	15.36	70.95	4.31	0.012
1.0	3.81	7.76	1.74	29.56	162.08	117.36	0.254
3.0	2.91	19.39	2.77	56.42	530.24	13,443.85	18.30

from 3.70 to 19.39 eV as nano-Y₂O₃ increased up to 3.0 wt%.

It was demonstrated in Wemple and DiDomenico model that the static refractive index at zero photon energy is given by [39, 51];

$$n_0^2 = \left(1 + \frac{E_d}{E_0} \right) \quad (5)$$

The values of n_0 tabulated in Table 1 and showed increase with the Y₂O₃ content. In addition, the dipole strength defined as $f = E_0 E_d$ and the estimated values show increase with increasing Y₂O₃ content (see Table 1).

It is important to estimate the linear optical susceptibility $\chi^{(1)}$ of PVA-Y₂O₃ films via the following relation [52];

$$\chi^{(1)} = \frac{E_d}{4\pi E_0} \quad (6)$$

Table 1 gives the values of $\chi^{(1)}$ that showed increase with the nano-Y₂O₃ content. Previous studies have shown

the possibility of calculating the third order optical susceptibility $x^{(3)}$ via Miller's rule like relation [53];

$$x^{(3)} = 6.82 \times 10^{-15} \left(\frac{E_d}{E_0} \right)^4 \text{ (e.s.u)} \quad (7)$$

In Table 1, the values of $x^{(3)}$ are given and shows increase as concentration of nano-Y₂O₃ increase up to 3.0 wt%. The nonlinear refractive index for the PVA-Y₂O₃ nanocomposite films described by the equation [54];

$$n_2 = \frac{12\pi x^{(3)}}{n_0} \quad (8)$$

Table 1 showed that the values of n_2 were enhanced when the concentration of nano-Y₂O₃ increased up to 3.0 wt%. By looking at previous research, we find that the values of nonlinear refractive index and third order optical susceptibility are greater than these found in the literature [55]. Hence, PVA-Y₂O₃ nanocomposite films can be used in applications of nonlinear optical devices.

The real and imaginary parts of optical dielectric constant are given in terms of refractive index and extinction coefficient as follows [16, 55, 56];

$$\begin{aligned}\epsilon_1 &= n^2 - k^2 = \epsilon_\infty - \frac{\omega_p^2}{\omega^2}, \\ \epsilon_2 &= 2nk = \frac{4\pi^2 e^2}{m^2 \omega^2 V} \sum_{v,c,k} |\Psi_k^v| p_i^{\rightarrow} |\Psi_k^c| \delta(E_{\Psi_k^c} - E_{\Psi_k^v} - hv)\end{aligned}\quad (9)$$

where ϵ_∞ denotes the high frequency dielectric constant, ω_p is the plasma frequency and Ψ_k^v defines the occupied but Ψ_k^c defines the unoccupied electronic states. The real optical dielectric constant ϵ_1 versus ω^{-2} of three compositions of PVA- Y_2O_3 films are plotted in Fig. 8.

As obtained from the figure above y-intercept equals ϵ_∞ and the slopes give the values of plasma frequency ω_p (see Table 2). It can be seen that the dielectric constants of the PVA- Y_2O_3 composites increase significantly with increasing Y_2O_3 content. For the PVA- Y_2O_3 nanocomposites, higher plasma frequencies achieved as the amount of Y_2O_3 in the composites increase.

From Eq. 9 when plotting ϵ_2 versus photon energy ($h\nu$) for the PVA- Y_2O_3 nanocomposite films (Fig. 9). The intercept of straight lines give the real energy gaps $E_{g(\epsilon_2)}$ which listed in Table 2. It was found that the values of $E_{g(\epsilon_2)}$ were

Table 2 Estimated values of ϵ_∞ , ω_p and the real energy gaps ($E_{g(\epsilon_2)}$) for the PVA- Y_2O_3 nanocomposite films

Y_2O_3 content (wt%)	ϵ_∞	$\omega_p \times 10^{14}$ (Hz)	$E_{g(\epsilon_2)}$ (eV)
0.0	2.12	7.30	5.25
1.0	3.69	12.32	5.23
3.0	12.05	32.81	5.20

5.41, 5.34 and 5.31 eV. Looking at Table 1 and comparing the energy gap values, it is found that the most probable transition is direct allowed.

As already mentioned, the optical conductivity (σ_{opt}) describes the response of medium to electromagnetic waves. To determine the optical conductivity we have to consider the relation between optical conductivity and refractive index given by [57, 58];

$$\sigma_{opt} = \frac{\alpha n C}{4\pi} \quad (10)$$

where C defines the speed of light in empty space. Figure 10 presents the optical conductivity data versus photon energy. The optical conductivity directly depends on refractive index and absorption coefficient of nanocomposites.

Fig. 8 Variation of ϵ_1 versus ω^{-2} for the PVA- Y_2O_3 nanocomposite films

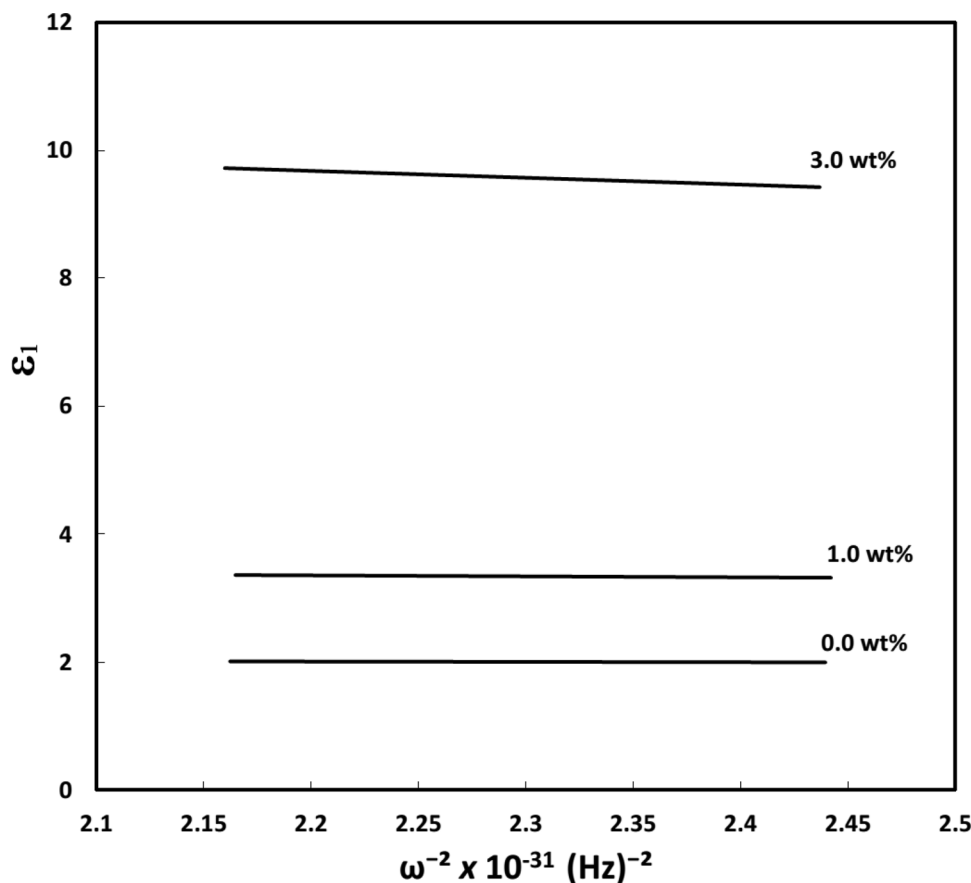


Fig. 9 Variation of ϵ_2 versus $h\nu$ for the PVA- Y_2O_3 nanocomposite films

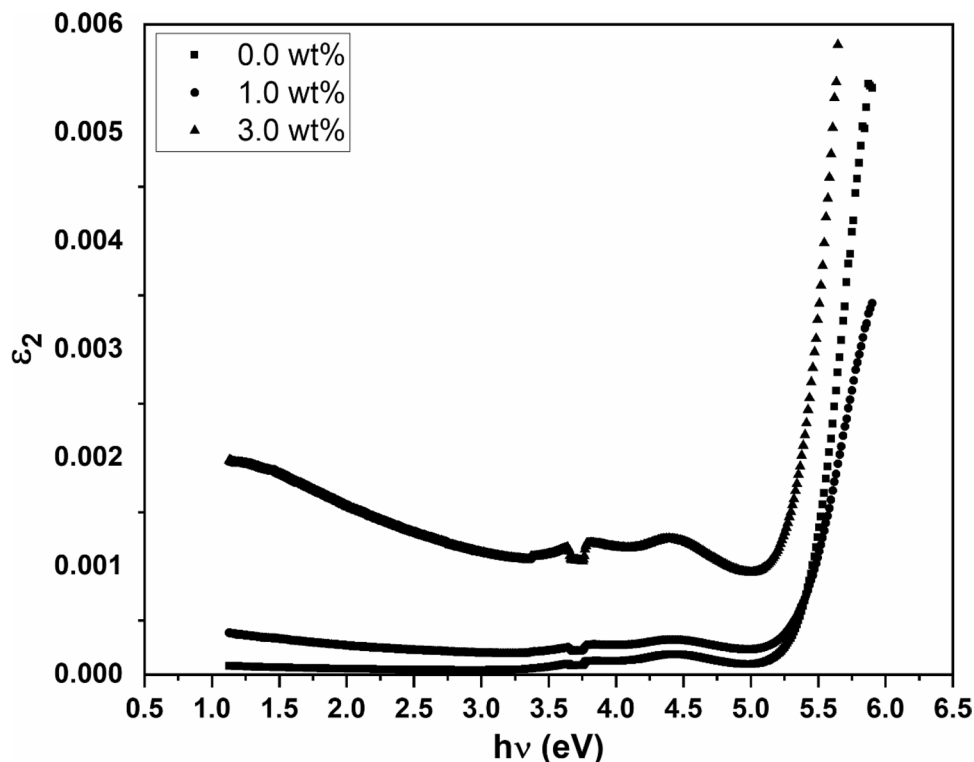
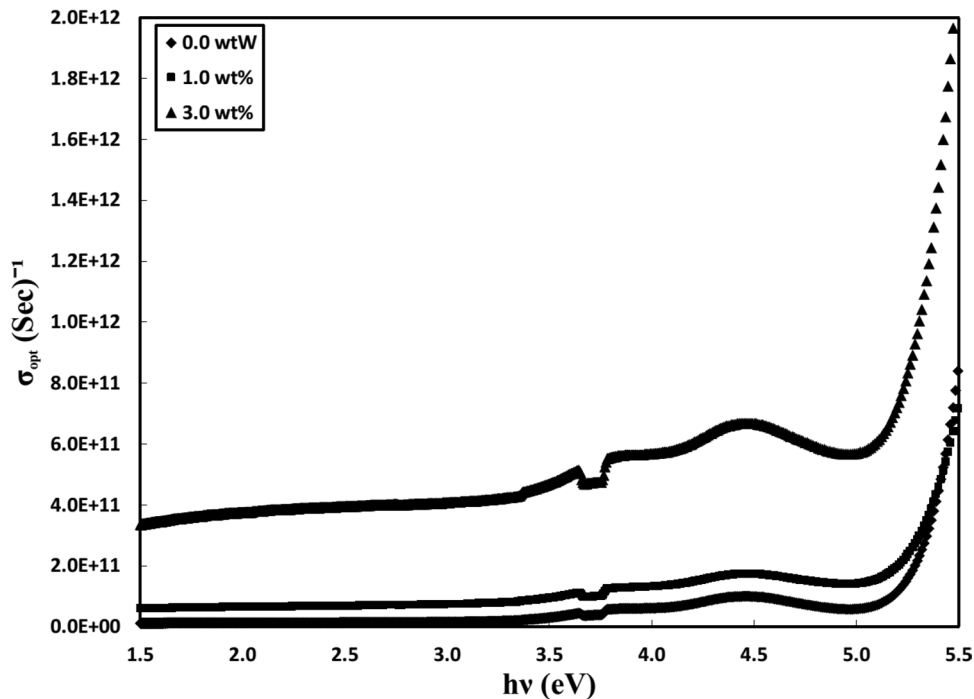


Fig. 10 Optical conductivity of the PVA- Y_2O_3 nanocomposite films as a function of photon energy



When the percent of Y_2O_3 and photon energy increase, the optical conductivities are increased significantly. This is probably due to the formation of new levels inside the band gap, which facilitate the excitation of electrons from

the valence band to the nearest states [55, 58]. These outcomes open the door for employing the prepared PVA- Y_2O_3 nanocomposite films in the optical and optoelectronic applications.

4 Conclusions

The effect of nano- Y_2O_3 on conventional PVA films have been examined by XRD, SEM, FTIR/ATR and optical absorption spectroscopy. The crystal structure of Y_2O_3 nanoparticles is cubic with an average crystal size of 28 nm. The dispersal of Y_2O_3 nanoparticles to the PVA polymer surface showed high uniform distribution. The FTIR spectra showed possible interactions between Y_2O_3 nanoparticles and host PVA films. Optical energy gaps at different concentrations of nano- Y_2O_3 decreased as the concentration reaches 3.0 wt%. The refractive index and optical dielectric constant of the nanocomposite films increased with an increase of Y_2O_3 in the polymer system. The dispersion energy, third order optical susceptibility, nonlinear refractive index and optical conductivity increased as well. Due to improvement in linear and nonlinear optical parameters, PVA- Y_2O_3 nanocomposite films can be applied in the optical and optoelectronic devices.

Acknowledgments The authors would like to extend their sincere appreciation to the Central laboratory at Jouf University for their support.

Declarations

Conflict of interest The authors declare that there is no conflict of interest.

References

1. Y.A. Hassan, H. Hu, Current status of polymer nanocomposite dielectrics for high-temperature applications. *Composites Part A* **138**, 106064 (2020)
2. M. Gong, L. Zhang, P. Wan, Polymer nanocomposite meshes for flexible electronic devices. *Prog. Polym. Sci.* **107**, 101279 (2020)
3. J. Loste, J.M. Lopez-Cuesta, L. Billon, H. Garay, M. Save, Transparent polymer nanocomposites: An overview on their synthesis and advanced properties. *Prog. Polym. Sci.* **89**, 133–158 (2019)
4. T.A. Taha, S.A. Saad, Processing, thermal and dielectric investigations of polyester nanocomposites based on nano- $CoFe_2O_4$. *Mater. Chem. Phys.* **255**, 123574 (2020)
5. T.A. Taha, N. Hendawy, S. El-Rabaie, A. Esmat, M.K. El-Mansy, Fluorescence and dielectric spectroscopy identification of polyvinyl chloride/NiO nanocomposites. *J. Mol. Struct.* **1212**, 128162 (2020)
6. A.S. Abouhaswa, T.A. Taha, Tailoring the optical and dielectric properties of PVC/CuO nanocomposites. *Polym. Bull.* **77**, 6005–6016 (2020)
7. B.P. Frank, D.G. Goodwin Jr., P. Bohutskyi, D.C. Phan, X. Lu, L. Kuwama et al., Influence of polymer type and carbon nanotube properties on carbon nanotube/polymer nanocomposite biodegradation. *Sci. Total Environ.* **742**, 140512 (2020)
8. M.B. Mohamed, M.H. Abdel-Kader, Effect of annealed ZnS nanoparticles on the structural and optical properties of PVA polymer nanocomposite. *Mater. Chem. Phys.* **241**, 122285 (2020)
9. T.A. Taha, S. Elrabaie, M.T. Attia, Exploring the structural, thermal and dielectric properties of PVA/ $Ni_{0.5}Zn_{0.5}Fe_2O_4$ composites. *J. Electron. Mater.* **48**(10), 6797–6806 (2019)
10. T.A. Taha, A. Hassona, S. Elrabaie, M.T. Attia, Dielectric spectroscopy of PVA- $Ni_{0.5}Zn_{0.5}Fe_2O_4$ polymer nanocomposite films. *J. Asian Ceram. Soc.* **8**(4), 1076–1082 (2020)
11. G.M. Aparicio, R.A. Vargas, P.R. Bueno, Protonic conductivity and thermal properties of cross-linked PVA/ TiO_2 nanocomposite polymer membranes. *J. Non-Cryst. Solids* **522**, 119520 (2019)
12. S. Ningaraju, A.G. Prakash, H.B. Ravikumar, Studies on free volume controlled electrical properties of PVA/NiO and PVA/ TiO_2 polymer nanocomposites. *Solid State Ionics* **320**, 132–147 (2018)
13. A. Kasikov, Optical inhomogeneity model for evaporated Y_2O_3 obtained from physical thickness measurement. *Appl. Surf. Sci.* **254**(12), 3677–3680 (2008)
14. H. Guo, Y.M. Qiao, Preparation, characterization, and strong upconversion of monodisperse Y_2O_3 : Er^{3+} , Yb^{3+} microspheres. *Opt. Mater.* **31**(4), 583–589 (2009)
15. A. Ubaldini, M.M. Carnasciali, Raman characterisation of powder of cubic RE_2O_3 ($RE = Nd, Gd, Dy, Tm, \text{ and } Lu$), Sc_2O_3 and Y_2O_3 . *J. Alloy Compd.* **454**(1–2), 374–378 (2008)
16. H. Donya, T.A. Taha, A. Alruwaili, I.B.I. Tomsah, M. Ibrahim, Micro-structure and optical spectroscopy of PVA/iron oxide polymer nanocomposites. *J. Mater. Res. Technol.* **9**(4), 9189–9194 (2020)
17. R.P. Chahal, S. Mahendia, A.K. Tomar, S. Kumar, SHI irradiated PVA/Ag nanocomposites and possibility of UV blocking. *Opt. Mater.* **52**, 237–241 (2016)
18. I. Morad, A.M. Alshehri, A.F. Mansour, M.H. Wasfy, M.M. El-Desoky, Facile synthesis and comparative study for the optical performance of different TiO_2 phases doped PVA nanocomposite films. *Physica B* **597**, 412415 (2020)
19. M. Rashad, Tuning optical properties of polyvinyl alcohol doped with different metal oxide nanoparticles. *Opt. Mater.* **105**, 109857 (2020)
20. M. Pattabi, A.B. Saraswathi, Optical properties of CdS–PVA nanocomposites. *Compos. Interfaces* **17**(2–3), 103–111 (2010)
21. G. Seeta Rama Raju, S. Buddhudu, A. Varada Rajulu, Red emission from Eu^{3+} : PVA polymer film. *J. Appl. Polym. Sci.* **102**(4), 3273–3276 (2006)
22. O.G. Abdullah, D.A. Tahir, K. Kadir, Optical and structural investigation of synthesized PVA/PbS nanocomposites. *J. Mater. Sci.: Mater. Electron.* **26**(9), 6939–6944 (2015)
23. Z.K. Heiba, M.B. Mohamed, N.G. Imam, N.Y. Mostafa, Optical and electrical properties of quantum composite of polyvinyl alcohol matrix with CdSe quantum dots. *Colloid Polym. Sci.* **294**(2), 357–365 (2016)
24. K.S. Hemalatha, K. Rukmani, N. Suriyamurthy, B.M. Nagabhushana, Synthesis, characterization and optical properties of hybrid PVA–ZnO nanocomposite: a composition dependent study. *Mater. Res. Bull.* **51**, 438–446 (2014)
25. K. Jayasankar, A. Pandey, B.K. Mishra, S. Das, Evaluation of microstructural parameters of nanocrystalline Y_2O_3 by X-ray diffraction peak broadening analysis. *Mater. Chem. Phys.* **171**, 195–200 (2016)
26. J.Y. Jeong, S.W. Park, D.K. Moon, W.J. Kim, Synthesis of Y_2O_3 nano-powders by precipitation method using various precipitants and preparation of high stability dispersion for backlight unit (BLU). *J. Ind. Eng. Chem.* **16**(2), 243–250 (2010)
27. T.A. Taha, A. Hassona, S. Elrabaie, M.T. Attia, Micro-structure, thermal, and dielectric performance of polyester nanocomposites containing nano- $Ni_{0.5}Zn_{0.5}Fe_2O_4$. *Appl. Phys. A* **126**(9), 1–10 (2020)

28. T.A. Taha, M.M. El-Molla, Green simple preparation of LiNiO₂ nanopowder for lithium ion battery. *J. Mater. Res. Technol.* **9**(4), 7955–7960 (2020)
29. T.A. Taha, A.A. Azab, E.H. El-Khawas, Comprehensive study of structural, magnetic and dielectric properties of Borate/Fe₃O₄ glass nanocomposites. *J. Electron. Mater.* **49**(2), 1161–1166 (2020)
30. M.H. Mahmoud, T.A. Taha, FTIR and Mössbauer spectroscopy investigations of Ag/Fe_xAl_{2-x}O₃ nanocomposites. *J. Electron. Mater.* **48**(11), 7396–7403 (2019)
31. Y. Yulizar, D.O.B. Apriandanu, J.L. Al Jabbar, Facile one-pot preparation of V₂O₅-Fe₂O₃ nanocomposites using *Foeniculum vulgare* extracts and their catalytic property. *Inorg. Chem. Commun.* **123**, 108320 (2021)
32. Y. Yulizar, D.O.B. Apriandanu, F.L. Hakim, Two-phase synthesis in n-hexane–water, characterization, and photocatalytic activity of ZnO/Bi₂Sn₂O₇ nanocomposite. *JOM* **73**(1), 441–449 (2021)
33. R.M. Surya, Y. Yulizar, A.H. Cahyana, D.O.B. Apriandanu, One-pot *Cajanus cajan* (L.) Millsp. leaf extract-mediated preparation of MgFe₂O₄ nanoparticles: optical, structural, morphological and particle size analyses. *Solid State Commun.* **326**, 114170 (2021)
34. H.A. Ariyanta, T.A. Ivandini, Y. Yulizar, Novel NiO nanoparticles via phytosynthesis method: Structural, morphological and optical properties. *J. Mol. Struct.* **1227**, 129543 (2021)
35. Y. Yulizar, A. Eprasatya, D.O.B. Apriandanu, R.T. Yunarti, Facile synthesis of ZnO/GdCoO₃ nanocomposites, characterization and their photocatalytic activity under visible light illumination. *Vacuum* **183**, 109821 (2021)
36. F.L. Hakim, Y. Yulizar, D.O.B. Apriandanu, Phase system of hexane-water for SnO₂ nanoparticles preparation using Cassia alata leaf extract and its photocatalytic activity. In IOP Conference Series: Materials Science and Engineering (Vol. 902, No. 1, p. 012016). IOP Publishing (2020)
37. K. Mustofa, Y. Yulizar, A. Saefumillah, D.O.B. Apriandanu, La₂O₃ nanoparticles formation using *Nothopanax scutellarium* leaf extract in two-phase system and photocatalytic activity under UV light irradiation. In IOP Conference Series: Materials Science and Engineering (Vol. 902, No. 1, p. 012018). IOP Publishing (2020)
38. T.A. Taha, A.A. Azab, M.A. Sebak, Glycerol-assisted sol-gel synthesis, optical, and magnetic properties of NiFe₂O₄ nanoparticles. *J. Mol. Struct.* **1181**, 14–18 (2019)
39. T.A. Taha, Z. Ismail, M.M. Elhawary, Structural, optical and thermal characterization of PVC/SnO₂ nanocomposites. *Appl. Phys. A* **124**(4), 307 (2018)
40. E.E. Abdel-Hady, H.F. Mohamed, M.O. Abdel-Hamed, M.M. Gomaa, Physical and electrochemical properties of PVA/TiO₂ nanocomposite membrane. *Adv. Polym. Technol.* **37**(8), 3842–3853 (2018)
41. D.O.B. Apriandanu, Y. Yulizar, CuO-bentonite-gold nanocomposites: Facile green preparation and their characterization. *Mater. Lett.* **284**, 128911 (2021)
42. A. Eprasatya, Y. Yulizar, R.T. Yunarti, D.O.B. Apriandanu, Fabrication of Gd₂O₃ nanoparticles in hexane-water system using *Myristica fragrans* Hoult leaves extract and their photodegradation activity of malachite green. In IOP Conference Series: Materials Science and Engineering (Vol. 902, No. 1, p. 012004). IOP Publishing (2020)
43. Putri, N., Yulizar, Y., Umar, A., & Apriandanu, D. O. B. (2020, July). Sm₂O₃ nanoparticles preparation using caesalpinia pulcherrima leaf extract, characterization and photocatalytic activity. In IOP Conference Series: Materials Science and Engineering (Vol. 902, No. 1, p. 012012). IOP Publishing.
44. Syahfitri, T. W. W., Yulizar, Y., Gunlazuardi, J., & Apriandanu, D. O. B. (2020, July). TiO₂/Co₃O₄ nanocomposite: Synthesis via *Catharanthus roseus* (L.) G. Don leaf extract, characterization and its photocatalytic activity for malachite green degradation. In IOP Conference Series: Materials Science and Engineering (Vol. 902, No. 1, p. 012003). IOP Publishing.
45. J.W. Rhim, C.K. Yeom, S.W. Kim, Modification of poly (vinyl alcohol) membranes using sulfur-succinic acid and its application to pervaporation separation of water–alcohol mixtures. *J. Appl. Polym. Sci.* **68**(11), 1717–1723 (1998)
46. C.P. Liu, C.A. Dai, C.Y. Chao, S.J. Chang, Novel proton exchange membrane based on crosslinked poly (vinyl alcohol) for direct methanol fuel cells. *J. Power Sources* **249**, 285–298 (2014)
47. Aziz SB, Hassan AQ, Mohammed SJ, Karim WO, FZ Kadir M, A Tajuddin H, NMY Chan N, Structural and optical characteristics of PVA: C-Dot composites: Tuning the absorption of ultra violet (UV) region. *Nanomaterials*, **9**(2), 216 (2019)
48. X. Xu, R. Lu, X. Zhao, S. Xu, X. Lei, F. Zhang, D.G. Evans, Fabrication and photocatalytic performance of a Zn_xCd_{1-x}S solid solution prepared by sulfuration of a single layered double hydroxide precursor. *Appl. Catal. B* **102**(1–2), 147–156 (2011)
49. N. Ghobadi, Band gap determination using absorption spectrum fitting procedure. *Int. Nano Lett.* **3**(1), 2 (2013)
50. F. Yakuphanoglu, H. Erten, Refractive index dispersion and analysis of the optical constants of an ionomer thin film. *Opt. Appl.* **35**(4) (2005)
51. I. Saini, J. Rozra, N. Chandak, S. Aggarwal, P.K. Sharma, A. Sharma, Tailoring of electrical, optical and structural properties of PVA by addition of Ag nanoparticles. *Mater. Chem. Phys.* **139**(2–3), 802–810 (2013)
52. B. Gündüz, Optical properties of poly [2-methoxy-5-(3', 7'-dimethyloctyloxy)-1, 4-phenylenevinylene] light-emitting polymer solutions: effects of molarities and solvents. *Polym. Bull.* **72**(12), 3241–3267 (2015)
53. F.A. Wahab, F. El-Diasty, M. Abdel-Baki, Dispersion dependence of second-order refractive index and complex third-order optical susceptibility in oxide glasses. *Phys. Lett. A* **373**(42), 3855–3860 (2009)
54. F. Yakuphanoglu, A. Cukurovali, I. Yilmaz, Determination and analysis of the dispersive optical constants of some organic thin films. *Physica B* **351**(1), 53–58 (2004)
55. T.A. Taha, N. Hendawy, S. El-Rabaie, A. Esmat, M.K. El-Mansy, Effect of NiO NPs doping on the structure and optical properties of PVC polymer films. *Polym. Bull.* **76**(9), 4769–4784 (2019)
56. F.M. Hossain, L. Sheppard, J. Nowotny, G.E. Murch, Optical properties of anatase and rutile titanium dioxide: Ab initio calculations for pure and anion-doped material. *J. Phys. Chem. Solids* **69**(7), 1820–1828 (2008)
57. J.I. Pankove, *Optical Processes in Semiconductors* (Dover Publications Inc., New York, 1975), p. 91
58. T.A. Taha, Optical properties of PVC/Al₂O₃ nanocomposite films. *Polym. Bull.* **76**(2), 903–918 (2019)

Publisher's Note Springer Nature remains neutral with regard to jurisdictional claims in published maps and institutional affiliations.